# Edinburgh Research Explorer

# Formation of extended ionomeric network by bulk polymerization of L,D-lactide with layered-double-hydroxide

# Formation of Extended Ionomeric Network by Bulk Polymerization of L,D-lactide with Layered Double Hydroxide

Edward D. McCarthy[a],  Mauro Zammarano[a, b, c] , Douglas M. Fox[c],  Ryan C. Nieuwendaal[a],  Yeon S. Kim[b], Paul H. Maupin[d] , Paul C. Trulove[e], Jeffrey W. Gilman[a*]

[a] Polymer Division, Material Measurement Laboratory, [b]Engineering Laboratory, National Institute of Standards and Technology (NIST), 100 Bureau Drive, Gaithersburg, MD 20899-8665, USA

[c] Department of Chemistry, American University, Washington DC, 20016, USA

[d] Chemical Sciences, Geosciences, and Biosciences Division Office of Basic Energy Sciences, Department of Energy, Washington, DC 20585-1290, USA

[e] Department of Chemistry, U.S. Naval Academy, Annapolis, MD, 21402-5026, USA

* Corresponding author. Tel: +13019756573; fax: +13019752091.
E-mail address: jeffrey.gilman@nist.gov

ABSTRACT.

We report the formation of an ionomeric network in a poly(L,D-lactide) hybrid nanocomposite, (PLDLA-HYB) during *in-situ* melt polymerization of L,D-lactide in the presence of magnesium/aluminium layered-double-hydroxide (LDH) without added catalyst.

The effect of LDH mass loading and reaction time on molecular mass and yield of soluble poly(L,D-lactide) (PLDLA-SOL) present in the hybrid was investigated for a better understanding of the conflicting roles of LDH in polymerization and degradation of PLDLA-SOL. High molecular mass PLDLA-SOL is obtained through initiation of polymerization by LDH. However an additional insoluble organic-inorganic fraction, INSOL, is also observed within the product when PLDLA-SOL is extracted using methylene chloride as solvent. It is proposed that INSOL is an ionomeric network comprising hydrogen-bonded, or otherwise co-ordinated, lactic acid monomer salts of magnesium, together with PLDLA in a 24 % to 76 % mass ratio.

KEYWORDS. Nanocomposite, polylactide, poly(lactic acid), layered double hydroxide, ionomer.

# INTRODUCTION

Ionomers are charge-bearing polymers, which are critical components of ionomeric polymer metal composites (IPMCs) and are used as actuators and sensors because of their characteristic electrical stimulus-response behavior, [1-3]. The advantages of such systems are their efficient use of energy and versatility of design and application. Use of IPMCs in artificial muscle tissue has been advanced as a target application [1]. In this paper we report the formation of an ionomer network in a two-phase poly(L,D-lactide) (PLDLA) hybrid nanocomposite.

Poly(lactic acid) (PLA) is one of the foremost modern examples of a fully renewable and biodegradable polymer produced in industrial quantities. Its life cycle begins with the photosynthesis of starch by plant material using sunlight, carbon dioxide and water [4, 5]. This starch is hydrolyzed in the presence of enzymes to produce lactic acid. The latter is then polymerized industrially to form poly(lactic acid) by either of two principal routes a) direct polycondensation of lactic acid molecules which produces water as an elimination by-product, or b) condensation of two lactic acid molecules to form a ring-structured lactide dimer, (L,D-lactide). Route b) is followed by ring-opening polymerization (ROP) of lactide to form high molecular weight PLA [6]. During ROP, the incipient polymer propagates by successive insertion of opened lactide rings at the first metal-oxygen bond of the polymer chain (Fig. 1b). ROP is industrially preferred for the production of high molecular mass PLA in high yield.

Ring-opening polymerization may occur by either of three principal routes: cationic (CROP), anionic, (AROP) and co-ordination insertion routes (CIROP) [6]. All three have been reported in the literature but the coordination-insertion ROP route has been developed industrially to the most advanced level [6-9]. This process usually employs either of two initiators: stannous octoate, which predominates, and aluminium isopropoxide, which is increasingly popular due to its relatively lower toxicity.

LDHs are layered anionic-exchangeable nanofillers that may occur naturally (*i.e.* hydrotalcite) or are synthesised industrially by co-precipitation of different inorganic salts. Their unique layered structure with high anionic exchange capacity allows them to host and release anionic compounds in a controlled fashion. They are used commercially as filler materials, fire retardants for polymer resins, drug delivery agents and catalyst supports [10-20]. Cationic-exchangeable nanofillers, like layered phyllosilicates, have been used for decades to prepare polymer nanocomposites. Blumstein *et al.* [21] prepared poly(methyl methacrylate) nanocomposites in 1961 and researchers at Toyota (with Unitika) produced polyamide-6/clay hybrids at an

industrial scale from the 1980s by *in-situ* polymerization [22]. The latter approach is significantly different from the standard physical processes of melt extrusion, which currently dominates the composite industry, and solvent intercalation of polymer into clay [23]. The potential to create strengthened polymeric-inorganic composite materials with phyllosilicates by *in-situ* polymerization has been demonstrated for poly(lactic acid) by Katiyar *et al.* [24]. Similarly, radical polymerization of methyl methacrylate has been achieved using a thermal radical initiator in the presence of 1 % by mass of stearate-intercalated LDH [23]. Additionally, lactide dimer was ring-open polymerized using stannous octoate in the presence of LDH, employing solution intercalation of the monomer, followed by *in-situ* polymerization of the monomer when fully intercalated [25].

However, there is also evidence in the literature that points to the role played by LDH in promoting depolymerization of poly(lactic acid) by inter- and intra-transesterification [26]. LDH may act as initiator for lactide polymerization promoting the formation of polylactide chains and can also promote main-chain scission. The interaction of these two mechanisms is poorly understood, and so affects the selection of appropriate processing conditions for maximal polymer yield and molecular mass.

Consequently, in this work it was decided to perform a polymerization of L,D-lactide using stearate-intercalated LDH (LDH), without any added solvent or initiator. This was to investigate whether LDH could be an effective initiator of L,D-lactide polymerization in its own right. The reaction resulted in major dissolution of the initial LDH and formation of a hybrid nanocomposite (PLDLA-HYB) comprising a soluble poly(L,D lactide) phase (PLDLA-SOL), and an insoluble network phase (PLDLA-INSOL). Both the overall PLDLA hybrid and its two phases are analyzed here. The insoluble phase is a supramolecular, ionic structure comprising hydrogen-bonded or otherwise co-ordinated lactic acid monomer salts of magnesium, together with PLDLA, in a 24 % to 76 % mass ratio.

## MATERIALS [1]

L,D-lactide monomer, stannous octoate initiator and 1-octanol coinitiator were obtained from Aldrich. Perkalite F100S, a stearate exchanged magnesium-aluminum LDH (Mg:Al ratio ≈ 2:1) with an interlayer d-spacing of 3 nm was obtained from Akzo-Nobel. L,D-lactide was sublimed and recondensed to remove moisture and stored in a desiccator over anhydrous calcium sulfate. LDH was dried *in vacuo* at 150 °C to remove moisture (about 11 % mass fraction) and was stored over anhydrous $CaSO_4$ when not immediately used. This was essential to prevent rapid re-adsorption of moisture. Both reagents were used as quickly as possible after both respective procedures.

## SAMPLE PREPARATION

**Control 1: Neat lactide.** 50 g of dried L,D-lactide was charged to a sealed, dry 100 ml PTFE vessel and purged with nitrogen. The pristine monomer sample was heated to 150 °C in a temperature-controlled Parr reactor at 1.1 bar and the reaction was allowed to proceed uninterrupted under mechanical stirring for 24 h. When the reaction was finished, the product was recovered from the vessel and stored in a desiccator.

**Control 2: Lactide with Stannous Octoate.** 50.0 g of dried L,D-lactide was charged to a sealed, dry 100 mL PTFE vessel and purged with nitrogen. After heating to 150 °C in a temperature-controlled oil bath, 34.7 µmol each of stannous octoate and 1-octanol were added by injection through a syringe port to start the polymerization and the reaction was allowed to proceed uninterrupted under magnetic stirring for 24 h. When the reaction was finished, the product (PLDLA-St-Oct-1%) was recovered from the vessel and stored in a desiccator.

**Control 3: Lactide with stearic acid, magnesium stearate or aluminum stearate.** 49.5 g of dried L,D-lactide and 1 % by mass (0.5 g) of stearic acid, magnesium or aluminum stearate salt were added to a sealed, dry 100 mL PTFE vessel, which was then purged with nitrogen. For each of the three polymerizations, the vessel was heated to 150 °C in a temperature-controlled Parr reactor and the reaction was allowed to proceed uninterrupted under mechanical stirring for 24 h. When the reaction was finished, the product was recovered from the vessel and stored in a desiccator.

---

**PLDLA-HYB**. PLDLA-LDH hybrid products (PLDLA-HYB) were obtained by heating various mixtures of L,D-lactide and layered double hydroxide at 150 °C for 24 h under mechanical stirring. Specifically, dried monomer and LDH were blended manually in a clean, dry PTFE vessel before the vessel was sealed, purged with dry nitrogen and pressured to 1.1 bar. The vessel was then immersed in a temperature-controlled Parr reactor fitted with agitator which was set at 100 rpm.

**Residual monomer extraction.** Following the reactions above, any unreacted lactide monomer and moisture were removed from the crude product *in vacuo* for 24 h at 130 °C. Primary samples of the crude product were reserved for TG analysis.

**Film preparation.** About 200 mg of PLDLA-LDH hybrid, pristine LDH-Stearate, lactic acid or were formed at a pressure of 1.55 MPa by a Carver press between Kapton films. LDH was cold-pressed at room temperature, polymeric compounds were hot-pressed above their respective melting temperatures (greater than 150 °C) and L,D-lactide monomer was pressed at just under its melting point (118 °C) to avoid extensive evaporation (120 °C plus).

**Separation of PLDLA-HYB into soluble and insoluble fractions by methylene chloride.** Methylene chloride was used to separate the soluble fraction (PLDLA) from the insoluble fraction (INSOL) of the PLDLA-LDH hybrids. The process consisted of three cycles of extraction and centrifugation where 0.5 g of product was dissolved in 20 mL of methylene chloride and centrifuged for 10 min at 1047 rad s$^{-1}$. Both fractions were dried at 60 °C for 12 h.

**METHODS**

Thermogravimetric analysis (TGA) was performed using a TA Q500 under nitrogen atmosphere at a temperature ramp rate of 10 °C/min. Isothermal thermogravimetry was performed at 150 °C with an initial heating ramp rate of 20 °C/min and average sample size of 3 mg. Infrared Spectroscopy in attenuated transmission reflectance mode (ATR-FTIR) was used (Thermo Nicolet Nexus 670) (spectra averaged over 128 scans, wavenumber range 600 cm$^{-1}$ to 4,000 cm$^{-1}$).

The soluble fractions of polymer melt products were analysed using gel permeation chromatography (GPC). A Waters system equipped with a 1515 isocratic high performance liquid chromatography HPLC pump, with online degassing, 717 Plus Autosampler, 2414 refractive index detector, a guard column, and three mixed bed columns (HR0.5, HR3 and HR4E) with 5 µm particle size was used. The HR0.5, HR3, and HR4E columns are

specified for molar mass separation range of (0 to $1.0 \cdot 10^3$) Da, ($5.0 \cdot 10^2$ to $3.0 \cdot 10^4$) Da, and ($5.0 \cdot 10^1$ to $1.0 \cdot 10^5$) Da, respectively. Tetrahydrofuran was the eluent at a flow rate of 0.35 mL / min, maintained at 30 °C, 4 mg/mL was the sample concentration where a 0.45 µm filter was used to exclude free clay particles and the injection volume was 40 mL.  A series of narrow polydispersity polystyrene standards were used to calibrate the GPC system and the results were adjusted for PLA polymer using a correlation based on the respective Mark-Houwink parameters of PLA and polystyrene, [27].

Scanning electron microscopy (SEM) of the freeze-fractured specimens was performed by a Zeiss Ultra 60 Field emission scanning electron microscope (Carl Zeiss Inc., Thornwood, NY). All SEM samples were sputter coated with 4 nm of Au/Pd (60 mass fraction %/40 mass fraction %) prior to SEM imaging.

Inductively-Coupled Plasma Optical Emission Spectrometry (ICP-OES) was performed by Galbraith Laboratories, Knoxville, TN, US. The X-ray diffraction experiments (XRD) were performed on a Rigaku Miniflex II  using a Cu $K_\alpha$ radiation ($\lambda = 0.15418$ nm) over a $2\theta$ range of 2º to 70º and at a scan rate of 0.50°/min. $2\theta$ measurements had an uncertainty of $2\theta = \pm 0.01°$.

Solid state $^{13}C$ {$^1H$} cross polarization magic angle spinning nuclear magnetic resonance (NMR) experiments were performed at 2.35 T (100 MHz) using a Tecmag Apollo console, ultrawide bore (125 mm) Nalorac magnet, and a custom-made double resonance 10-mm magnetic angle spinning probe. Typical parameters were $\upsilon_c = 25.19$ MHz, $\upsilon_H = 100.16$ MHz, 3.5 µs $^1H$ $\pi/2$ pulse, 2 ms contact pulse, $B_1(H) = 62$ kHz, $B_1(C) = 66$ kHz,  4 kHz MAS, 78 kHz cw $^1H$ decoupling, 100 µs dwell time, 600 data points, 60 ms acquisition window, 16k scans, and 3s recycle delay. Adamantane was used for Hartman-Hahn optimization and served as an external $^{13}C$ chemical shift reference.

**RESULTS AND DISCUSSION**

A schematic of sample preparation, extraction and mass balance of species is shown in Figure 2 for the case of PLDLA-HYB-5% produced from the reaction of 95 % by mass L,D-lactide and 5 % by mass LDH. L,D-lactide was melt polymerized *in-situ* in the presence of LDH at three different reaction times (30 min, 4 h and 24 h) and five mass ratios of lactide to LDH (99:1, 95:5, 90:10, 85:15 and 80:20).

The ATR-FTIR spectra of the hybrid containing 5 % by mass of LDH reacted for 24 h (PLDLA-HYB-5%), L,D-lactide and LDH are shown in Figure 3. The features observed in the PLDLA-HYB-5% spectrum are typical for PLA [27]. These include peaks at 1750 cm$^{-1}$ (C=O) 1444 (CH$_3$ bend) and (1180, 1080 and 1040) cm$^{-1}$ (C-O stretch). Furthermore, there is a clear distinction between the spectrum for L,D-lactide and the product melt, most notably the absence of the ring strain signal at 929 cm$^{-1}$. The characteristic peaks of LDH (carboxylic hydroxyl peak at 3421 cm$^{-1}$, and carbonate peaks at 1542 and 1460 cm$^{-1}$) are almost completely absent from that of the hybrid. These spectra imply that a substantial conversion of L,D-lactide to PLDLA is obtained and that LDH structure is substantially altered.

TGA was used to measure the percent polymer mass yield. The TGA samples were heated isothermally for 4 h in nitrogen at 150 °C and their residual masses were measured. Lactide monomer and first-order LDH moisture are completely eliminated at this time and temperature as shown in Figure 4. The percent polymer mass yield vs. initial LDH content is shown in Table 1. The polymer yield is maximal at 5 % by mass of LDH but decreases with increased LDH loading. Possibly, the degradation function of LDH dominates that of initiation resulting in lower net polymer yield. Poor mixing at higher melt viscosity, caused by increased LDH loading may also reduce monomer conversion, through reducing the amount of lactide molecules which contact initiation sites.

In Figure 5 a GPC chromatograph of L,D lactide self-polymerized in bulk by polycondensation (L,D lactide 24) is compared to PLDLA-SOL-5 %-24h, and PLDLA-2.5 %-Mg-Stearate and PLDLA-2.5 %-Al-Stearate (i.e. L,D-lactide polymerized with stearate mass loading level equivalent to a loading of 5 % LDH by mass).

The self-polymerized lactide shows a low molecular mass distribution centered at approximately $9 \cdot 10^2$ Da. Mg-Stearate is an effective initiator for ROP polymerization [8]. Mg-Stearate-initiated polymerization here (Fig. 5) produced PLDLA with molecular mass fractions up to $2 \cdot 10^4$ Da. However, Al-Stearate is even more effective, producing PLDLA with a high molecular mass peak at $5.5 \cdot 10^4$ Da, which is not seen in PLDLA

2.5% Mg-Stearate. The PLDLA-2.5 %-Al-Stearate distribution also shows a slight shoulder in proximity to the Mg-Stearate principal peak, indicating a secondary population of shorter-chain PLDLA. The latter could be the result of a secondary, less dominant polymerization mechanism. However, it is unclear from GPC analysis alone which mechanism is dominant; whether CIROP, AROP or another process.

LDH-polymerized L,D-lactide shows molecular-mass-distribution peaks centered at approximately $8.5 \cdot 10^3$ Da and $5 \cdot 10^4$ Da. It is clear that the LDH-mediated reaction achieves markedly higher molecular mass, which ROP by Mg-stearate anion alone cannot generate. This suggests that at least one additional polymerization mechanism occurs in the presence of LDH. The high molecular mass peak of PLDLA-SOL-5% is very similar to that produced by the Al-Stearate control reaction, which strongly suggests that aluminum moieties within the LDH may be responsible, although it is not clear whether the aluminum-initiated route is predominantly CIROP or AROP. CIROP of L,D-lactide by a combination of a cation and anion have been shown to initiate PLDLA ROP in the literature [7, 8]. LDH provides both the cationic moieties (*i.e.*, $Mg^{2+}$ and $Al^{3+}$) and anionic moieties (*i.e.*, stearate and hydroxyl anions). We propose that LDH promotes lactide polymerization by a combination of CIROP and AROP mechanisms (Fig. 1). The bimodal distribution observed for PLDLA-SOL-5% suggests that there are two polymerization mechanisms and possibly also a competing de-polymerization mechanism, which is limiting the molecular mass. The two polymerization mechanisms could be differentiated as AROP and CIROP. However it is also possible that the magnesium and aluminum of the LDH are associated with two separate polymerization processes progressing at different rates and producing PLDLA chain populations of differing molecular mass distributions.

In Figure 6 GPC chromatographs of soluble fractions at loadings of 5 %, 10 % and 20 % by mass of LDH are shown. PLDLA molecular mass distribution is affected by LDH loading. The highest molecular weight, with a peak at approximately $5 \cdot 10^4$ Da, is obtained with 5 % by mass LDH. This is the same LDH loading level that gave the highest polymer yield as measured by TGA (Fig 5a). LDH is effectively promoting lactide polymerization up to a critical loading level (about 5 % by mass). However, LDH can also promote PLDLA de-polymerization [26] and our results show that above this critical concentration this effect may be predominant. Another possible explanation is that, as already mentioned, LDH acts as an initiator for ROP so that the average molecular mass of the polymer might decrease with an increase in LDH content due to the increase in the number of initiation sites.

Thus three explanations can be put forward to account for this bimodal characteristic:

1.	Aluminum stearate moieties in the LDH are responsible for initiating high molecular mass material, based on the molecular mass distribution (MMD) determined for the PLDLA 2.5% Al-Stearate control. The aluminum stearate reaction may have faster polymerization kinetics than the equivalent reaction initiated with Mg-Stearate, resulting in longer PLDLA chains over the same reaction period. The high molecular mass peak generated by the PLDLA 2.5% Al-Stearate control would support this argument.  The peak of the MMD observed for magnesium stearate is over an order of magnitude smaller, though still higher than values reported for Mg-Stearate by Kricheldorf *et al.*, [8].

2.	The lower molecular mass observed could be a consequence of initial space restriction within the LDH-St interlayers during the first 2 h of reaction (c.f. molecular mass distributions Figure 7 a, b), whereas higher molecular mass PLDLA chains would be formed in free melt regions of the mixture where no such spatial restrictions exist. Disassembly of the LDH structure with reaction time would further facilitate the formation of higher molecular mass PLDLA chains, a phenomenon we discuss below.

3.	The molecular mass distribution could represent an equilibrium: between polymerization by both methods, and PLDLA degradation by moisture and/or by LDH-St.

Another important question was the extent to which reaction time affects the average molecular mass. Figure 7 shows the molecular mass distributions versus molecular mass for three soluble fractions derived from three separate reactions at different reaction times. Molecular mass distribution is initially mono-modal at 30 min for masses in excess of $5.0 \cdot 10^2$ Da. However, at 2 h two principal changes are observed: a) the peak of the lower molecular mass distribution (LMMD) shifts left from $1.1 \cdot 10^4$ to $6.5 \cdot 10^3$ Da, possibly due to chain hydrolysis and b) a second shoulder appears at higher molecular mass between $2.0 \cdot 10^4$ g mol$^{-1}$ and $3.0 \cdot 10^4$ Da which becomes a more intense and predominant peak after 24 h at $5.0 \cdot 10^4$ Da. This is accompanied by a progressive reduction in intensity of the LMMD peak, indicating that a second polymerization mechanism becomes progressively more dominant after 2 h of reaction. Possibly, spatial restriction for polymer chain growth disappears as the LDH layer structure is disassembled, which may account for the sudden shift in the molecular mass distribution from low to high mass material between 2 h and 24 h, (Figure 7). This transition from unimodal to bimodal molecular mass distribution would seem to suggest that spatial restriction is the decisive factor affecting the distribution of PLDLA chain lengths. Spatial restriction may also have contributed to the predominance of low molecular mass PLA observed by Chiang et al., [26].

Certainly, the appearance of this secondary fraction of high molecular mass material after 2 h does not support the idea that degradation of PLDLA by LDH in any way dominates processes in the reaction system during this period. Figure 8 shows the total polymer yield of three separate PLDLA-HYB-5% reaction products derived at different reaction times from 30 min to 24 h. Here it is clear that there is an increase in polymer yield from 62 % at 30 min to 75 % at 2 h to 88 % at 24 h. Clearly, polymerization progresses over time although an effect of LDH on de-polymerization cannot be excluded.

**Separate Analyses of PLDLA-SOL and INSOL after Extraction of Annealed Product.**

It was believed that LDH could initiate the polymerization of lactide at the surface of LDH platelets and in the interlayers of LDH galleries to form a brush-type covalently-bonded hybrid, (Fig. 1). If this were correct, it would be possible to extract excess soluble polymer from the primary melt and measure any increase in mass in the insoluble residue due to tethered chains on LDH platelets. PLDLA is soluble in methylene chloride but LDH is insoluble; hence it was thought any significant increase in insoluble material would be caused by species grafted to LDH. Thus, the primary product was extracted with methylene chloride and the soluble extract and insoluble residue fractions were characterized separately to understand what polymerization and/or degradation mechanisms had contributed to the formation of either fraction. A similar extraction was performed on PLDLA 2.5% Al-St as a control, (PLDLA 2.5% Al-St INSOL). An insoluble gel of PLDLA-2.5%-Al-St was also extracted which comprised 7 % by mass of the product. The mass balance of PLDLA-HYB 5 % before the reaction and after separation of the reaction product into soluble and insoluble fractions by extraction is shown in Figure 2. The total percent polymer yields for the hybrid products and the total insoluble fractions after extraction for each are shown in Table 1.

Here, a definite effect of initial LDH fraction is seen: an insoluble mass residue of 9.1 % is obtained at 1 % LDH by mass, which increases by a factor of 2.5 to 24.4 % when 5 % by mass LDH is used. More notably, the proportion of insoluble to soluble polymer continues to increase even as the total polymer yield itself decreases at 10 % LDH concentration, (41.5 % of the polymer insoluble). This trend is then reversed at 15 % LDH, (34.3 % by mass insoluble polymer), and finally falls to a value of 18.5 % insoluble at 20 % LDH. It is possible that the ratio of insoluble to soluble polymer could be correlated with the ratio of PLDLA chains initiated at fixed LDH gallery initiation sites by ROP to those initiated in the free melt by free anions. Such anions could be stearate anions displaced into the free melt from LDH sites by lactate anions, (Fig. 1c).

It may be that as LDH concentration increases, restrictions on the ability of available lactide monomer to diffuse into the clay galleries, in addition to steric hindrance of growing PLA chains at the edge of LDH platelets, may be the limiting factors in determining the initiation and growth of PLA chains, regardless of the number of initiation sites on the LDH. If this is the case, diffusion becomes the limiting process at a critical LDH concentration between 5 % and 10 % by mass. However, further increase in LDH concentration has only a marginal additional effect in limiting monomer conversion. It is also possible that increased availability of surface initiation sites on LDH platelets could compensate for the increased melt viscosity and diffusion barrier to interlayer ROP caused by increased LDH concentration. In addition, the decrease in absolute monomer concentration at higher LDH loading would explain the lower average molecular masses observed.

The two fractions were then analyzed using TGA to determine the balance of organic and inorganic material. Figure 9 shows thermogravimetric mass loss curves for PLDLA-SOL-5% samples and reactant controls: a) the pristine lactide monomer, b) pristine LDH, c) the primary melt product (PLDLA-HYB-5%), d) PLDLA-INSOL-5%, the residue of the melt product after extraction with methylene chloride, (24.4 % by mass), e) PLDLA-SOL-5%, the corresponding soluble fraction of the methylene chloride extract, (75.6 % by mass), and f) PLDLA-St-Oct-1%, the PLDLA product produced from polymerization using stannous octoate initiator.

Pristine undried LDH has an inorganic mass fraction of 28.3 %. Upon drying, LDH loses 11 % by mass of moisture and the residual inorganic mass fraction is 31.8 % at 800 °C. The PLDLA-HYB-5% product has a final residue of 3.3 % by mass at the same temperature. There is an expected inorganic residue of 0.05 x 0.318 = 1.6 % by mass. However, the product has a surplus black residue of 1.9 % by mass, which can be attributed to carbonaceous char. The persistence of this material at 800 °C indicates some form of strong interaction or bonding between the respective organic and inorganic residues. This evidence supports the idea that LDH directly initiates L,D-lactide polymerization in a manner which creates a brush-type graft of PLDLA on LDH platelets.

PLDLA-INSOL-5% shows a persistent 16.3 % by mass inorganic residue determined at 800 °C, implying a substantial organic fraction of 83.7 % by mass. This further confirms the substantial and strong attachment of organic material to the final inorganic residue of the original LDH at elevated temperature consistent with some form of chemical bonding or brush polymerization. Lastly, PLDLA-St-Oct-1% has practically no residue at 800 °C, consistent with absence of LDH and/or cross-linked moieties.

Both of these TGA results provide substantial evidence that comprehensive and strong interaction of LDH with organic species exists. To determine the chemical nature of both fractions they were analyzed by FTIR-ATR. Figure 10 shows FTIR of the soluble polymer contrasted with that of the insoluble residue obtained during the same extraction process and pristine LDH. Both the insoluble and soluble fraction spectra show evidence of the methylene stretching peaks at 2920 $cm^{-1}$ and 2850 $cm^{-1}$ indicating a certain concentration of stearic acid and/or stearate salt in both soluble and insoluble polymer fractions, but these are more pronounced in the spectrum of PLDLA-SOL-5%. There is also almost complete agreement between the other peaks of the two spectra which are characteristic of PLDLA [28]. However, one key difference is the peak at 1650 $cm^{-1}$, which is far more intense in the insoluble fraction spectrum when compared to the soluble polymer spectrum. This peak is relatively close to a 1634 $cm^{-1}$ signal attributed to both interlayer and adsorbed water molecule bending modes within hydrotalcite [29, 30] possibly indicating the presence of residual moisture in the residue. However, a signal of 1650 $cm^{-1}$ may also be assigned to stretching modes of carbonate moieties [31]. It is possible that small levels of atmospheric carbon dioxide were reabsorbed into the original LDH reactant which were then converted to carbonates and partially displaced some stearate gallery anions by ion exchange.

The metal elemental compositions of PLDLA-SOL-5% and PLDLA-INSOL-5% were determined using inductively-coupled plasma spectrometry to obtain further chemical characterization, particularly with regard to the ratio of magnesium to aluminum in PLDLA-INSOL-5% relative to LDH as the comparative control for the analysis.  Results are shown in Table 2.

Firstly, the mass ratios of magnesium to aluminum in LDH closely corresponds to the classical 2 : 1 ratio found in the formula for the synthetic clay i.e. 2.2 : 1 .  However, the most dramatic comparison in these results is the contrast between the magnesium / aluminum ratio of LDH and PLDLA-INSOL-5%. Here, the ratio changes from 2.2 : 1 to 11 : 1 demonstrating a dramatic deficiency of aluminum in the insoluble product relative to LDH. This demonstrates that the octahedral sheet structure of the clay must have been comprehensively dissolved. It also implies that the balance of aluminum absent from PLDLA-INSOL-5% must be present in PLDLA-SOL-5%, so that it is likely that aluminum was the dominant partner in the ROP mechanism with stearate anion displaced in anion exchange with dilactate. The aluminum depletion in PLDLA-INSOL-5% indicates that the L, D lactide polymerization phenomenon coincides with, if it does not directly cause, the disintegration of the LDH structure.

A selection of SEM images were taken to elucidate the morphology and microstructure of reactants and PLDLA hybrid products (Figs. 11 & 12). In Figure 11 a) the rosetta-like-structure morphology of the pristine LDH can be directly contrasted with the amorphous structure of a pristine poly(L,D-lactide) matrix polymerized using stannous octoate catalyst, PLDLA-1%-StOct (Fig. 11 b)). Both these morphologies are in stark contrast to the long, laminar plate morphology clearly visible in PLDLA-HYB-10%, (Fig. 12 a-c). The equivalent image for the gel extract, (7 % by mass), of PLDLA 2.5% Al Stearate is provided in Fig. 11 c). This is clearly an amorphous, continuous surface without clear evidence of crystallinity or network structure.

The SEM images of the initial reactants may be contrasted with a selection of scanning electron micrographs of the insoluble residue. Figures 13 a) – c) show the residues of the three melt products PLDLA-INSOL-1, -5 and -10% after extraction of soluble PLDLA with methylene chloride. In Figure 13 a) a mixture of randomly distributed rosetta platelets and amorphous material is evident which may indicate the coexistence of PLDLA with persistent LDH.

However, the corresponding images for PLDLA-INSOL-5% and -10 % (Fig. 13 b and c) are of a completely different character to that of PLDLA-INSOL-1%, showing the existence of a three dimensional network of material resembling  PLDLA, (Fig. 11 b), interspersed with platelets resembling LDH (Fig. 11 a). The formation this network coincides with the disappearance of the LDH morphology and implies the migration of LDH moieties into a continuous molecular structure which incorporates both lactic acid moieties and the metal cations of LDH. The CIROP process which creates grafted polymer-cation hybrids would facilitate this. Finally, Figure 14 shows SEM images of PLDLA-INSOL-5% at three magnifications demonstrating the pervasive nature of the network throughout the sample.

Having established the network morphology of the insoluble residue on a micro-scale, the molecular structure was investigated, including any crystallinity, using X-ray diffraction. The X-ray powder diffraction spectra for the pristine LDH and three PLDLA-INSOL-5% reaction residues of separate reaction hybrids are shown in Figure 15.

The pristine LDH is characterized by a broad peak at 3.1 nm (Fig. 15a i). This first-order peak represents the interlayer d-spacing between LDH sheets and demonstrates a broad distribution of this spacing size throughout the sample [32]. Second and third order overtones of this peak are visible with peaks at approximately 1.52 nm and 1.0 nm, respectively. The fourth principal feature is a peak centered at approximately 0.44 nm, which is either a primary signal of the crystal structure or a third overtone of the

interlayer spacing at 3.08 nm. Lastly, a defined peak at 0.165 nm is visible which may be attributed to an average value of the (Mg-O / Al-O) bond spacings in the clay sheet molecular structure. Normally, the typical linear bond spacings of the Mg-O and Al-O bonds are quoted as 0.175 nm [32], and between 0.18 nm to 0.20 nm [33] in the literature respectively. Thus, it is clear that the octohedral arrangement of the LDH gallery reduces this average bond distance considerably. Indeed such bond shortening of the Al-O bond is explicitly recognized in [34] for an Al-O bond within a group of aluminum alkoxides $AlH_2OR$, (R = H, $CH_3$), and the values reported frequently approximate 0.165 nm as reported here.

Clearly, the three residue spectra are substantially different in character from the pristine LDH; firstly, there is a near total elimination of the broad interlayer peak around 3.1 nm, which is more pronounced for the two reaction residues at 4 h and 24 h. This indicates that the LDH has been almost completely disordered at this size scale. Secondly, an array of peaks unique to the residue appear in the size range 0 nm to 1 nm with one large peak centered between 0.92 nm and 0.95 nm, a second centered between 0.509 nm and 0.512 nm, and at least nine other significant peaks in the size domain 0.2 nm < d < 0.48 nm. The primary and secondary peaks at 0.9 nm and 0.5 nm could be attributed to the lengths of particular salt molecules such as magnesium lactate, with individual bond lengths represented by the peaks at locations lower than 0.2 nm. However, it would be necessary to perform single-crystal X-ray diffraction to more exactly identify these spacings and deduce an exact crystal structure. Overall, the fundamental difference in the diffraction signatures of the pristine clay and the set of three residue samples indicates a comprehensive difference in structure between them at molecular level. In particular the severe depletion of the Mg-O and Al-O peak region at 0.165 nm, (Fig. 15b ii), suggests substantial molecular disassembly of the octahedral molecular sheet. This evidence, together with the significant reduction in aluminum concentration in the residue established by bulk elemental analysis, indicates that the pristine clay has been comprehensively disassembled during the polymerization of the lactide dimer.

The close correspondence of the XRD peaks from the residue with those from literature for magnesium lactate [35], (Fig. 15a v), suggests that the latter salt comprises a high proportion of the residue left after extraction. This is because at least nine close signal matches are achieved between the lactate salt and the reaction residue, with a similar correspondence of relative peak intensities.

A number of other magnesium and aluminum salt controls were also tested to investigate whether they might be present in the residual network structure. These were aluminum and magnesium stearate respectively, as

well as aluminum lactate. The stearate and lactate salts were of particular interest; the first because of the presence of stearic acid in the initial layered double hydroxide and the second, because it was suspected that lactate salts might form between the gallery cations and any lactate anions derived from ring-opened lactide dimer. However comparison of these three salts' diffraction spectra, (Fig. 16 v – vii), with that of the residue (Fig. 16 ii – iv) showed little or no correspondence.

The number of close peak matches between magnesium lactate and the reaction residue strongly supports the case for the formation of a supramolecular residue structure comprising PLA and monomeric magnesium lactate salts co-ordinated and stabilized with each other by strong ionic interaction. The XRD peaks of size 0.95 nm or less are of the correct order of magnitude to represent features of a magnesium lactate molecule.

A number of $^{13}$C NMR spectra of key reaction products, residues and soluble polymer extracts were obtained to investigate the structures resulting from the LDH *in-situ* polymerization. In particular, it was desired to identify the respective end-group structures of PLDLA within the residue and soluble fractions. A comparison of the principle spectra is provided in Figure 17. Each polymer-based spectrum (Figure 17 i-iii) features the standard signature peaks of neat, non-crystalline PLDLA polymer at approximately (17, 69, and 170) ppm, representing the methyl, methine and ester-carbonyl carbon shifts, respectively [36-38]. Furthermore, the LDH-polymerized PLDLA-SOL-5% spectrum (Figure 17 iii) exhibits a methylene resonance at 29.8 ppm, which is due to terminal stearate groups. The methylene resonance is 7.2 % of the intensity of the methine resonance. Since there are sixteen methylene carbons per stearate molecule, this suggests there is on average one stearate molecule per 220 lactide monomer units (approx $3.2 \cdot 10^4$ Da) which agrees quite well with the GPC data for PLDLA-SOL-5%.

In Figure 17 iv, the spectrum for the PLDLA-INSOL-5 % exhibits resonances at (15.4, 68 and 168.4) ppm, indicating the presence of PLDLA. The stearate methylene resonance (29.7 ppm) observed in PLDLA-INSOL-5% (which, again, is presumably due to PLDLA chain ends) is approximately 7.5 % of the intensity of the PLDLA methyl resonance (15.4 ppm), which suggests there is on average one stearate group per 230 lactide groups very similar to the soluble PLDLA fraction. In addition, the residue exhibits unique carbonyl resonances at 180.4 ppm and 182.5 ppm, which represent the shifts of two salt-type carbonyl-moieties, as well as a pair of downfield methyl resonances (21.4, 20.0 ppm) and an overlapping shoulder on the methine resonance (66.8 ppm). Similar carbonyl, methine, and methyl features are observed in the control spectrum for magnesium lactate salt (Figure 17 v), which strongly suggest the presence of magnesium lactate in the residue

in addition to PLDLA. These two downfield carbonyl resonances (180.4 ppm, 182.5 ppm) are 19 % of the total carbonyl intensity by integration, and the two downfield methyl resonances (21.4 ppm, 20.0 ppm) are 20 % of the total methyl intensity. This suggests that the residue consists of approximately 20 % magnesium lactate salt and 80 % PLDLA by mol% of lactide monomer, noting that the NMR spectrum intensity estimate is quantitative to approximately 10 %. This agrees qualitatively with the 86 % / 16 % mass ratio of organic to inorganic material established from TGA of PLDLA-INSOL-5%, (Figure 9 d).

The aluminum lactate control spectrum (Figure 17 vi), exhibits a single, broad downfield carbonyl shift at 178.8 ppm. The negligible intensity at 178.8 ppm in the residue spectrum (Figure 17 iv) strongly suggests that the insoluble residue contains a negligible amount of aluminum lactate salt. This is supported by the 11:1 ratio of magnesium to aluminum established by ICP-OES for PLDLA-INSOL-5% (Table 2) and the good correspondence of X-ray diffraction data between magnesium lactate and the insoluble residue.

**Conclusions**

An *in-situ* polymerization of L,D lactide monomer took place in the presence of LDH, and the polymer yields were of the same order of magnitude as those achieved with conventional catalysts such as stannous octoate. The initial LDH concentration had a definite effect on the polymer yield, and two populations of polymeric species, $CH_2Cl_2$-soluble and insoluble were present This is consistent with the operation of both anionic ring opening polymerization, AROP, in the free melt and coordination insertion polymerization, CIROP, at initiation sites on the LDH octahedral sheets. The formation of a magnesium lactate network in the insoluble fraction is also indicated.

The insoluble residues (PLDLA-INSOL) of the reaction showed network morphology, which was dependent on the initial concentration of LDH employed in the polymerization. Isothermal TGA of PLDLA-INSOL-5% indicated an organic : inorganic mass ratio of 84 : 16  indicating significant persistence of organic material in the residue despite thorough extraction with methylene chloride. This organic material has been identified using Xray and ^{13}C NMR as a magnesium lactate supra-molecular complex, which forms during the *in-situ* polymerization.

The formation of an ionomeric network in place of the layered double hydroxide has important implications for industrial extruder processes, which mix LDHs with polymers such as poly(lactide) since cycles of PLDLA decomposition and repolymerization can be established. As a result, the processing characteristics of

this system are currently being investigated using melt rheology so as to better understand the contribution of such insoluble networks to overall mechanical properties of these polymer nanocomposite melts.

Perhaps more importantly, this and similar lactone-based systems could be considered as sustainable substitutes for ionomeric polymer-metal composite (IPMC) systems used in electro-actuator applications. This aspect of the system merits further investigation.

## References

1. Nemat-Nasser S, Thomas CW, Chapter 6: Ionomeric Polymer-Metal Composites, in Bar-Cohen Y, Electroactive Polymer Actuators as Artificial Muscles: reality, potential and challenges, SPIE Press Monograph, Washington DC, 2004

2. Chen Z., Tan X., Sensors and Actuators A 157 (2010) 246–257

3. Liua S, Montazamic R, Liua Y, Jain V, Lin M, Zhoua X, Hefline JR, Zhanga QM, Sensors and Actuators A 157 (2010) 267–275

4. Garlotta D. J Polym Env, 2010; 9, 63-84.

5. Nampoothiri KM, Nair RN, Rojan PJ. Bioresource Technology, 101, 2010; 8493 – 8501.

6. Kricheldorf HR, Chemosphere 2001; 43, 49-54.

7. Kricheldorf HR, Kreiser-Saunders I. Makromol Chemie, 1990; 191, 1057-1066.

8. Kricheldorf HR, Serr A, Polymer Bulletin, 1985, 14, 497-502

9. Kricheldorf  HR, Dunsing R. Makromol. Chemie 1986; 187, 1611-1625.

10. Shibasaki Y, Sanada H, Yokoi M, Sanda F, Endo T. Macromolecules 2000; 33, 4316-4320.

11. Kricheldorf HR, Kreiser-Saunders I, Stricker A. Macromolecules 2000; 33, 702-709.

12. Oh J.M, Park CB, Choy JH. J Nanosci Nanotechnol 2011; 11, 1632-5.

13. Li Y, Liu D, Ai H, Chang Q, Liu D, Xia Y, Liu S, Peng N, Xi Z, Yang X. Nanotechnology 2010; 21, 105101.

14. Xu ZP, Walker TL, Liu K, Cooper HM, Lu GQM, Bartlett PF. Int. J. Nanomedicine, 2007; 2 163–174.

15. Gunawan P, Xu R. J Pharm Sci, 2008; 97, 4367-78.

16. Brito, ME Borges, M Garn, A Hernandez. Energy Fuels, 2009; 23, 2952–2958.

17. Sharma YC, Sing B, Korstad J. Fuel 2011; 90, 1309–1324.

18. Unnikrishnan R, Narayanan S. Journal of Molecular Catalysis A, 144, 173-179.

19. Choudary BM, Madhi S, Chowdari NS, Kantam ML, Sreedhar B. J. Am. Chem. Soc., 2002;124, 14127-36.

20. Raja T, Jyothi TM, Sreekumar K, Talawar MB, Santhanalakshmi J, Rao BS. Bull Chem Soc Jpn, 72, 2117 – 2119.

21. Blumstein, Bull. Chem. Soc. Jpn, 1961; 899

22. Okada M, Kawasumi A, Usuki Y, Kojima T., Kurauchi O, Kamigaito. In: D.W. Schaefer, J.E. Mark, editors. Polymer based molecular composites. MRS Symp. Proceedings, Pittsburgh 1990; 171, 45–50.

23. Nogueira T, Botan R, Wypych F, Lona L. Composites: Part A, 2011; 42, 1025–1030.

24. Katiyar V, Nanavati H, Polymer Composites, 2011; 32, 497

25. Katiyar V, Gerds N, Koch CB, Risbo JH, Hansen CB, Plackett D. Polym. Degrad. Stab., 2010; 95, 2563-2573.

26. Chiang MF, Chu MZ, Wu TM. Polym. Degrad. Stab., 2011; 96, 60-66.

27. Yu Y, Storti G, and Morbidelli M. Macromolecules 2009; 42, 8187–8197.

28. Braun B, Dorgan JR and Dec SF. Macromolecules 2006; 39, 9302-9310.

29. Ureña-Amate MD, Boutarbouch ND, del Mar Socias-Viciana M, González-Pradas E. Applied Clay Science, 2011; 52, 368–373.

30. Palmer SJ, Grand LM, Frost RL. Spectrochimica Acta, Part A , 2011; 79, 156–160.

31. Arihara K., Kitamura F., Ohsaka T., Tokuda K., J. Electr. Chem. 510 (2001) 128–135

32. Jain, KV, Sluiter M, Kawazoe Y. Computational Materials Science 2006; 36, 171–175.

33. Barron AR, Dobbs KD, Francl MM. J. Am. Chem. Soc. 1991; 113, 39-43.

34. Evans DG, Slade RC. Struct Bond 2006; 119: 1–87.

35. Smith JV, Beward AS, Berry LG, Post B, Weissmann S., eds., 'X-ray Powder Data File, Sets 1-5", ASTM Special Technical Publication 48-J, p. 16, Item I-0061, 1961.

36. Espartero JL, Rashkov I, Li SM, Manolova N, Vert M. Macromolecules 1996; 29, 3535-3539.

37. Zell MT, Padden BE, Paterick AJ, Thakur KAM. Macromolecules 2002; 35, 7700-7707.

38. Suganuma K, Horiuchi K, Matsuda H, Cheng HN, Aoki A, Asakura T. Macromolecules 2011; 44, 9247-9253

**FIGURES**
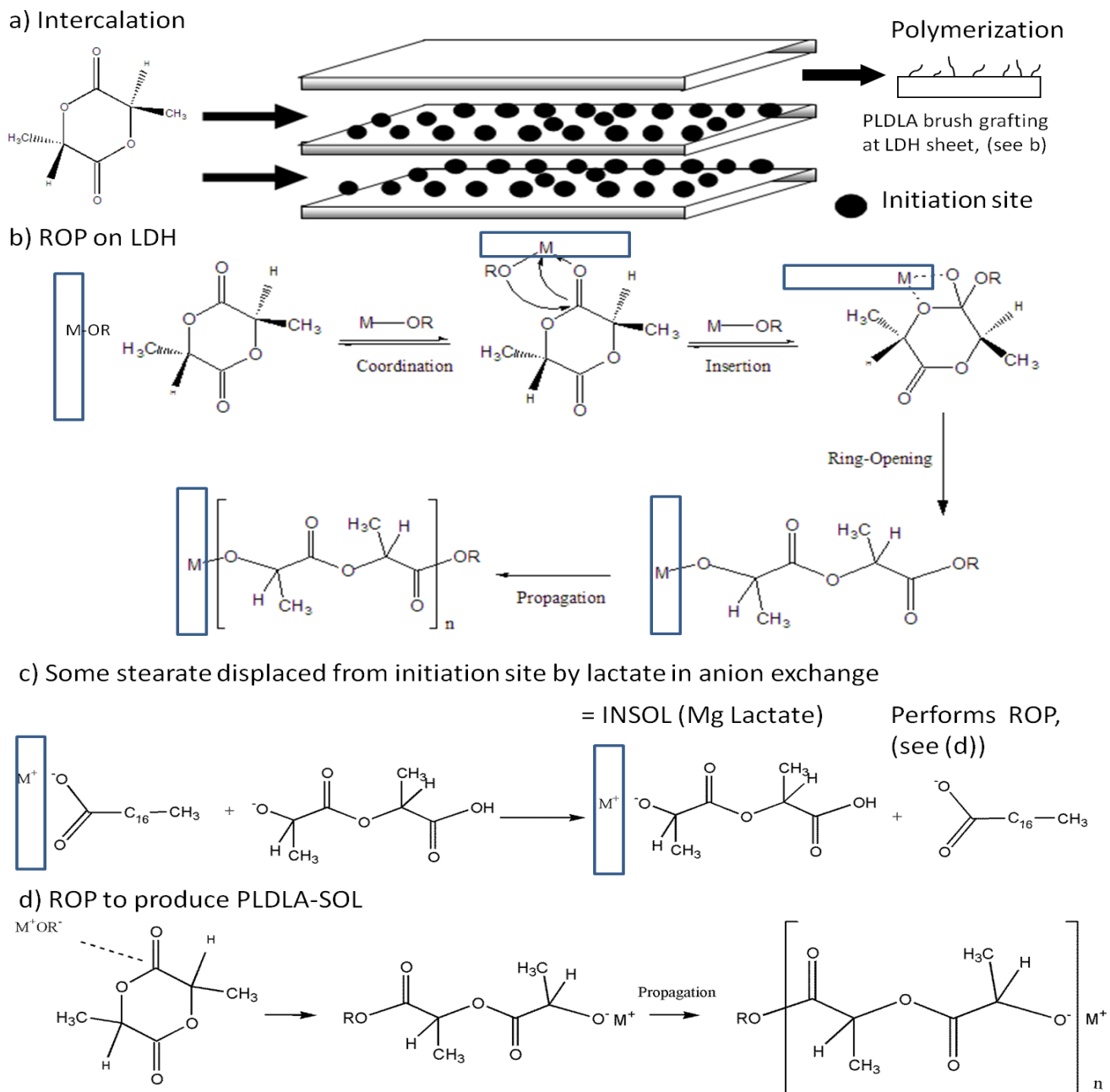


Figure 1 (a) Schematic of initial LDH, (Mg Al LDH-St), interlayer intercalated with stearate anions; lactide dimers intercalate between layers and are polymerized at both the exchanged stearic acid anion sites, and by free stearate anions, released by ion exchange with other lactate anions at the initiation sites. (b) Co-ordination-insertion ROP process, [5-8, 25].
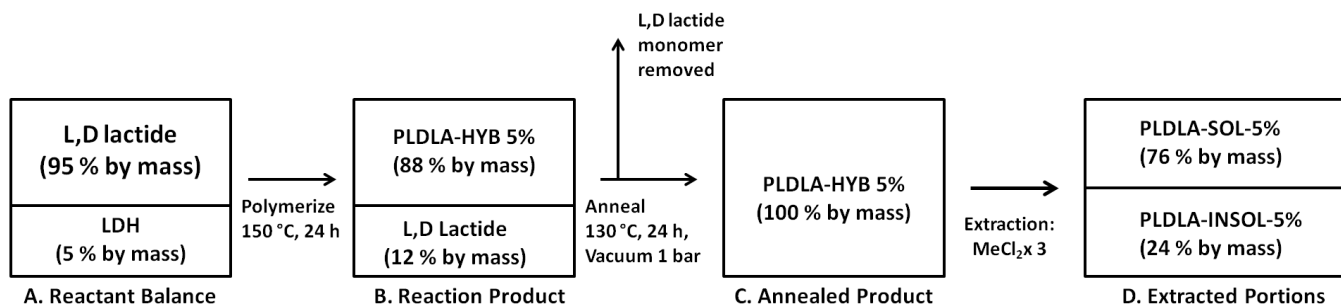
**Figure 2 Process scheme and mass balances for PLDLA-HYB-5% and its fractions after extraction with methylene chloride, (mass % from thermogravimetric analyses of species).**
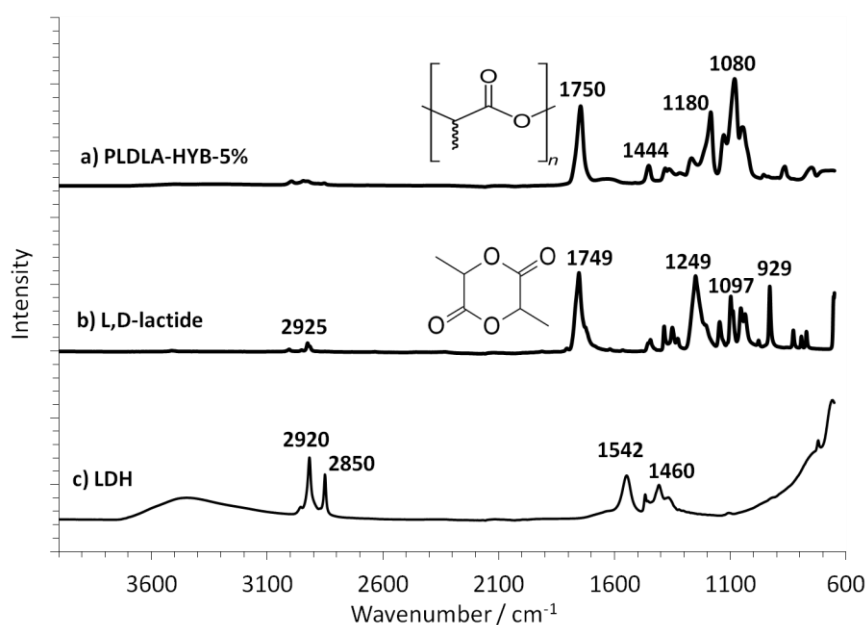


**Figure 3 Fourier Transform Infrared Signals for a) PLDLA-HYB-5% b) L, D lactide monomer and c) LDH. The spectrum for a) PLDLA-HYB-5% is that of a polylactide, with an absence of the characteristic L,D lactide peak at 929 cm⁻¹. Characteristic PLDLA peaks occur at 1750 cm⁻¹, (C=O), 1444, (CH₃ bend) and (1180, 1080 and 1040) cm⁻¹, (C-O stretch).**
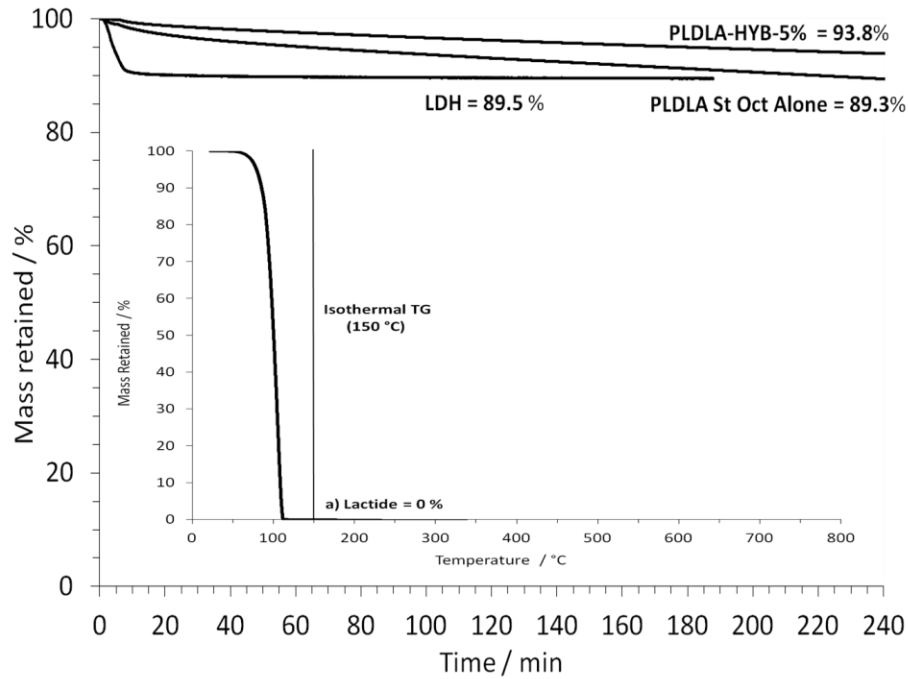
**Figure 4 Isothermal TG of undried LDH, PLA Stannous Octoate and PLDLA-HYB-5% at 150 °C, with (inset); L,d lactide depletion at 150 °C, (dynamic TG measurement).**
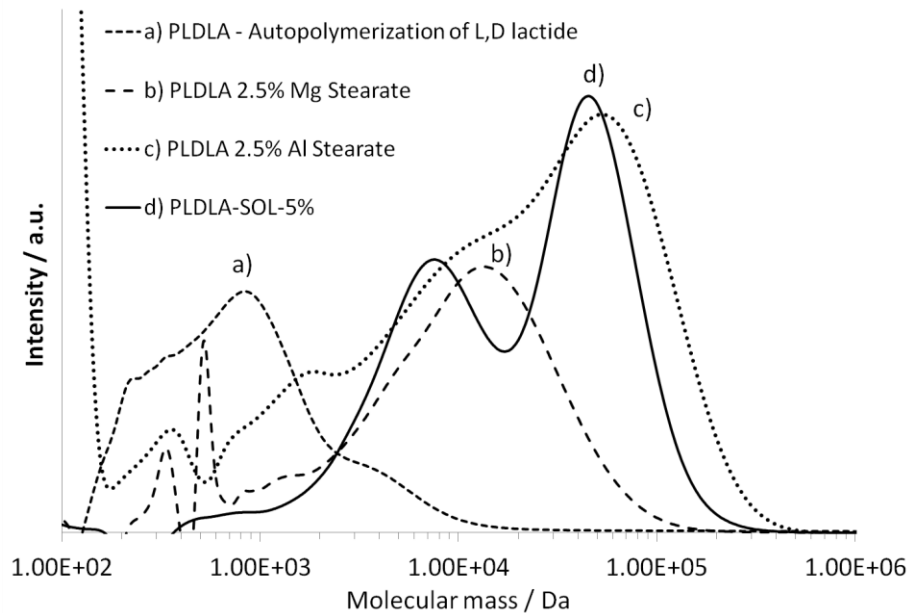


**Figure 5 Gel permeation chromatographs of (a) lactide autopolymerisation product, (b) PLDLA Mg Stearate c) PLDLA Al Stearate and (d) soluble extract of PLDLA-HYB-5%.**
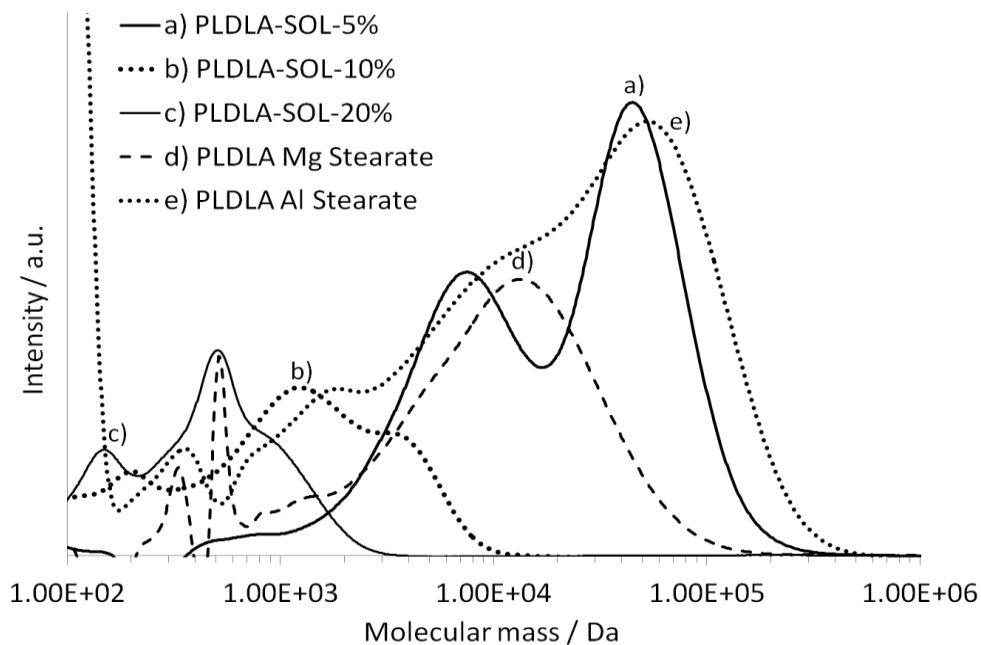
**Figure 6 Gel permeation chromatographs of a) PLDLA-SOL-5%, b) -10% and c) -20% extracted from annealed hybrid products compared with that for d) PLDLA-Mg-Stearate and e) PLDLA Al Stearate alone.**
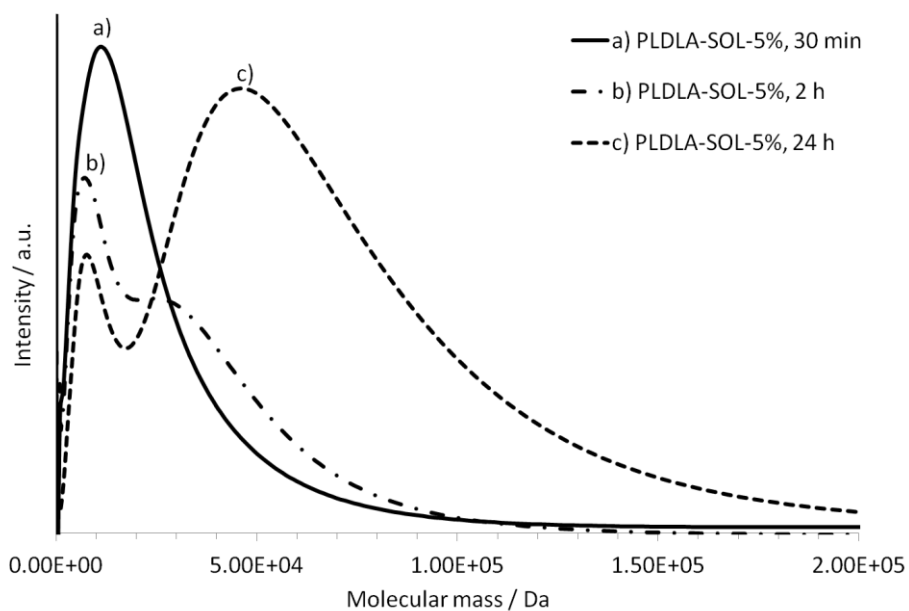


**Figure 7 Gel permeation chromatographs of PLDLA-SOL-5% extracted from different PLDLA-HYB-5% products reacted for a) 30 min, b) 2 h and c) 24 h respectively.**
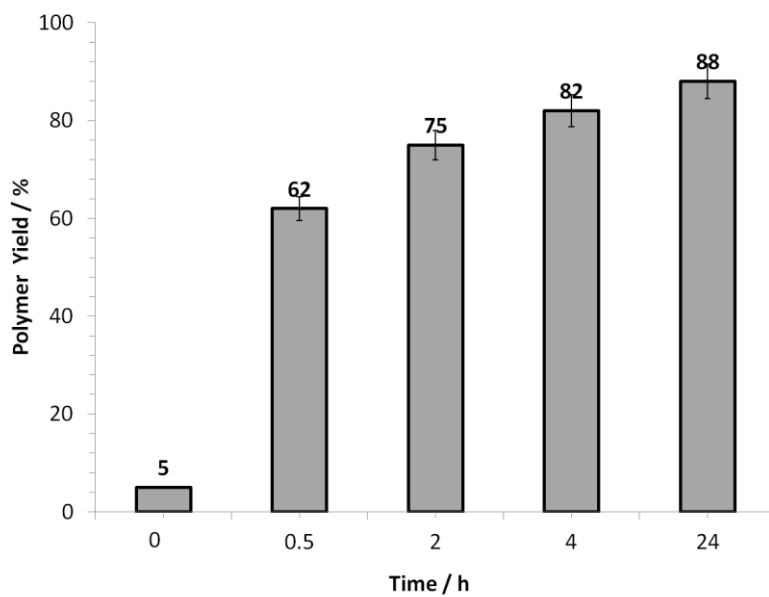
**Figure 8 Total polymer mass yield of the PLDLA-HYB-5% reaction product as a function of reaction time, (different reactions), as determined by isothermal TGA at 150 °C. (Error bars: ± 2 %)**
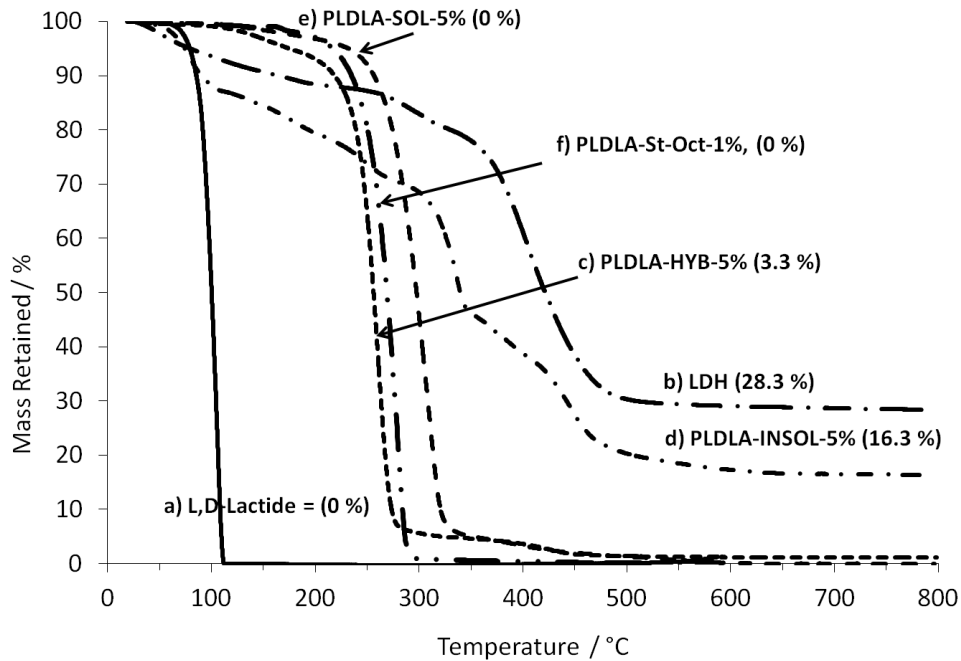
**Figure 9 Thermogravimetric curves for a) the pristine lactide monomer, b) pristine LDH, c) PLDLA-HYB-5%, d) PLDLA-INSOL-5%, (24.4 % by mass), e) PLDLA-SOL-5% (75.6 % by mass of HYB), f) PLDLA 1% St Oct. (% mass residues at 800 °C in brackets)**
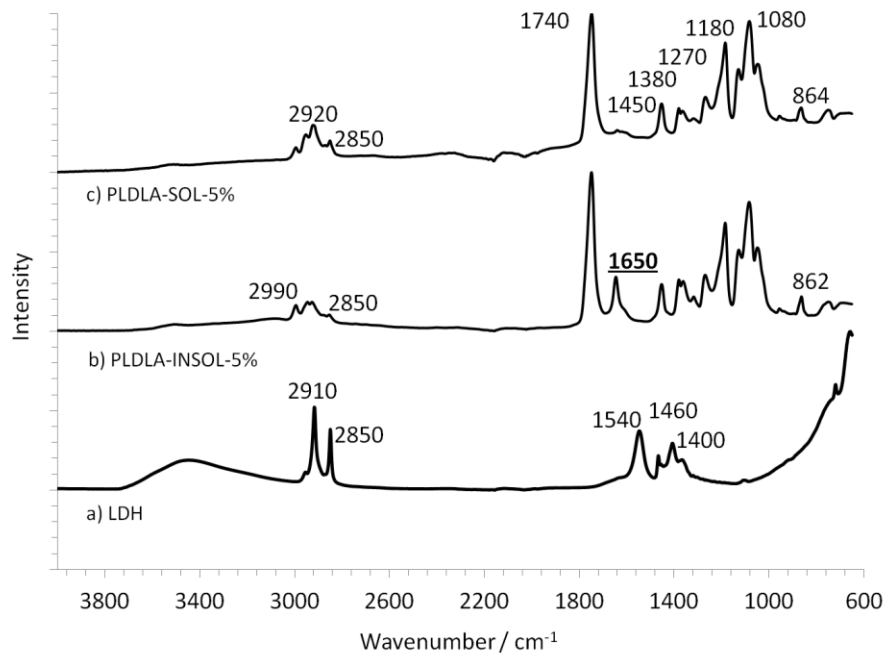


**Figure 10 FTIR-ATR Spectra of Soluble and Insoluble fractions of PLDLA-HYB-5%**
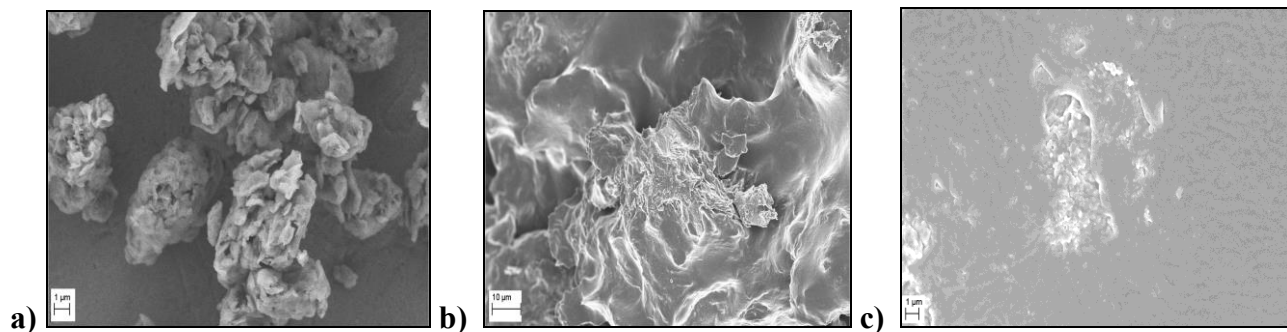
**Figure 11 SEMs of a) LDH, b) PLDLA-1%-St-Oct  c) PLDLA 2.5% Al-St-INSOL**
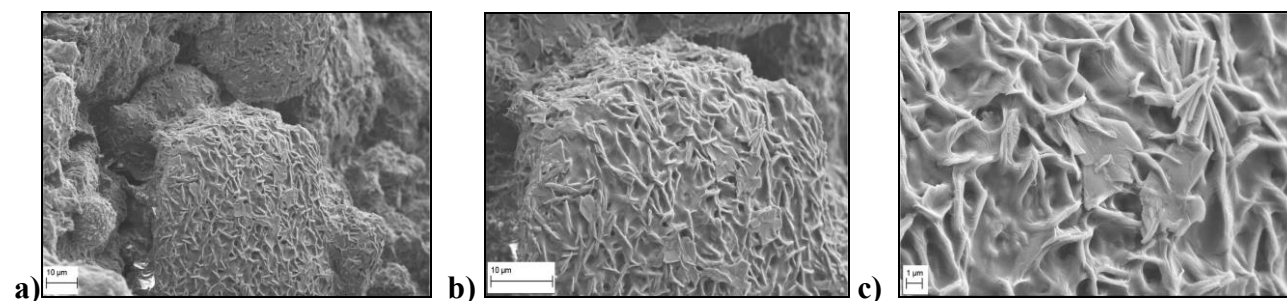


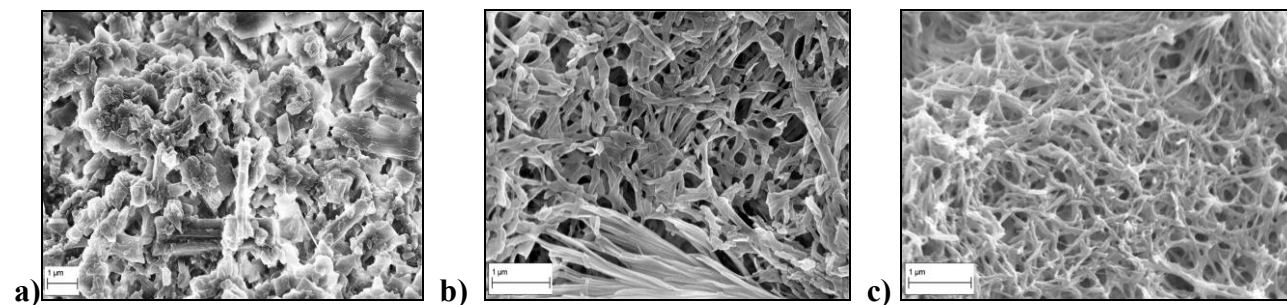**Figure 12. Scanning electron micrographs of PLDLA-HYB-10%; a) x10K, b) x 20K, c) x 100K**



**Figure 13. Scanning electron micrographs of a) PLDLA-INSOL-1%, b) -5% and c) -10%,  at magnifications of 100,000X, 200,000X and 200,000X respectively**
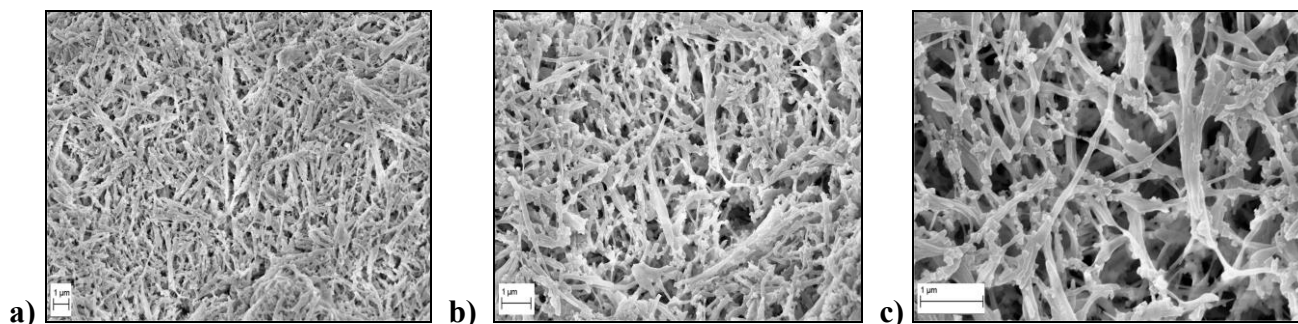


**Figure 14 Scanning electron micrographs of PLDLA-INSOL-5% at magnifications of a)  50,000X, b) 100,000X and c) 200,000X respectively.**
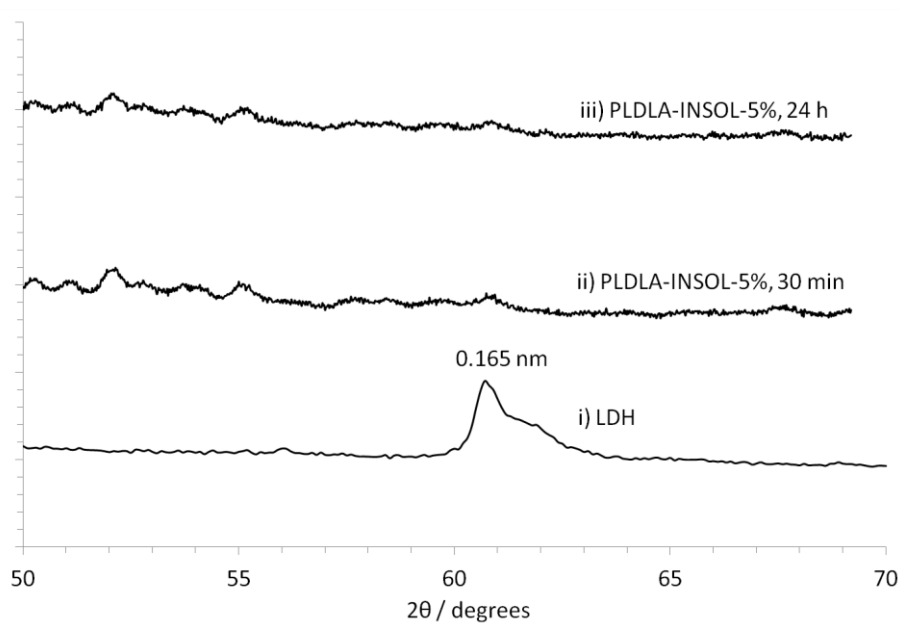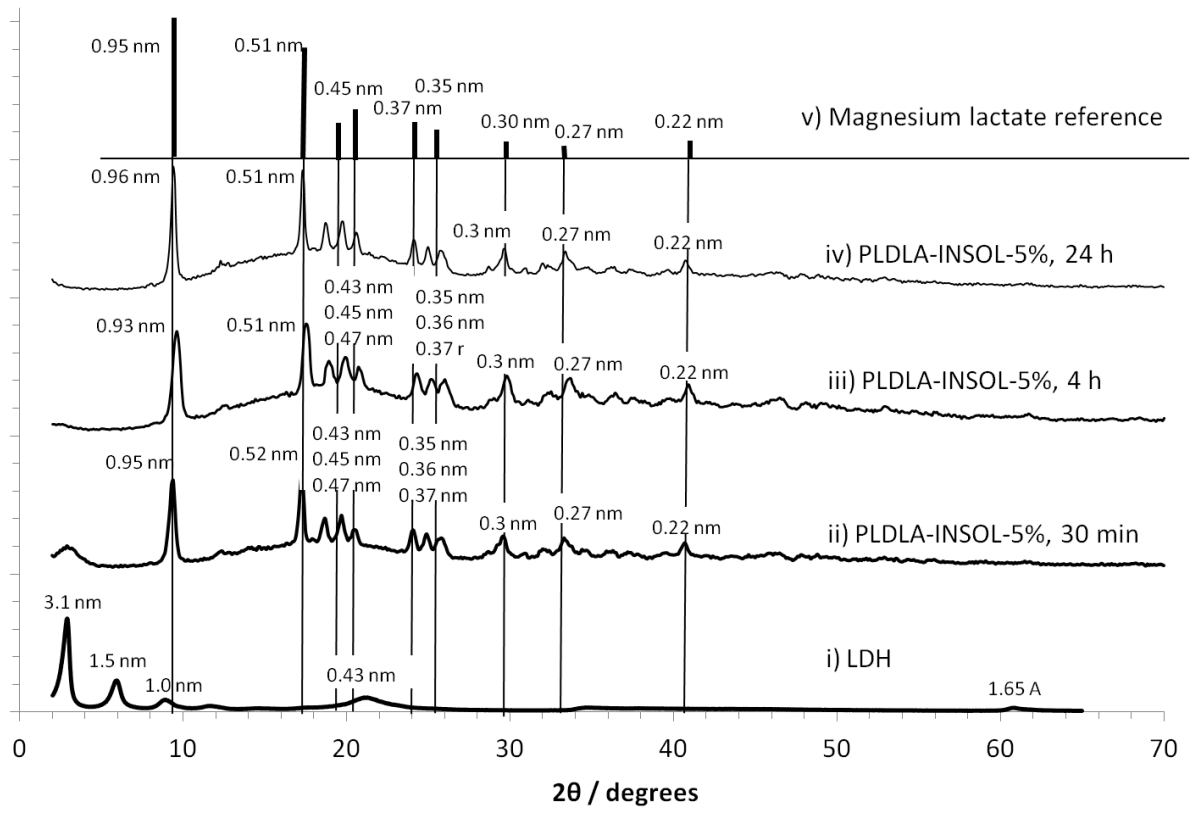
28

**Figure 15 a) Xray diffraction spectra of PLDLA-INSOL-5% compared with that of LDH and magnesium lactate peaks from reference, [25]. b) selected curves from 50° - 70°, (2θ)**
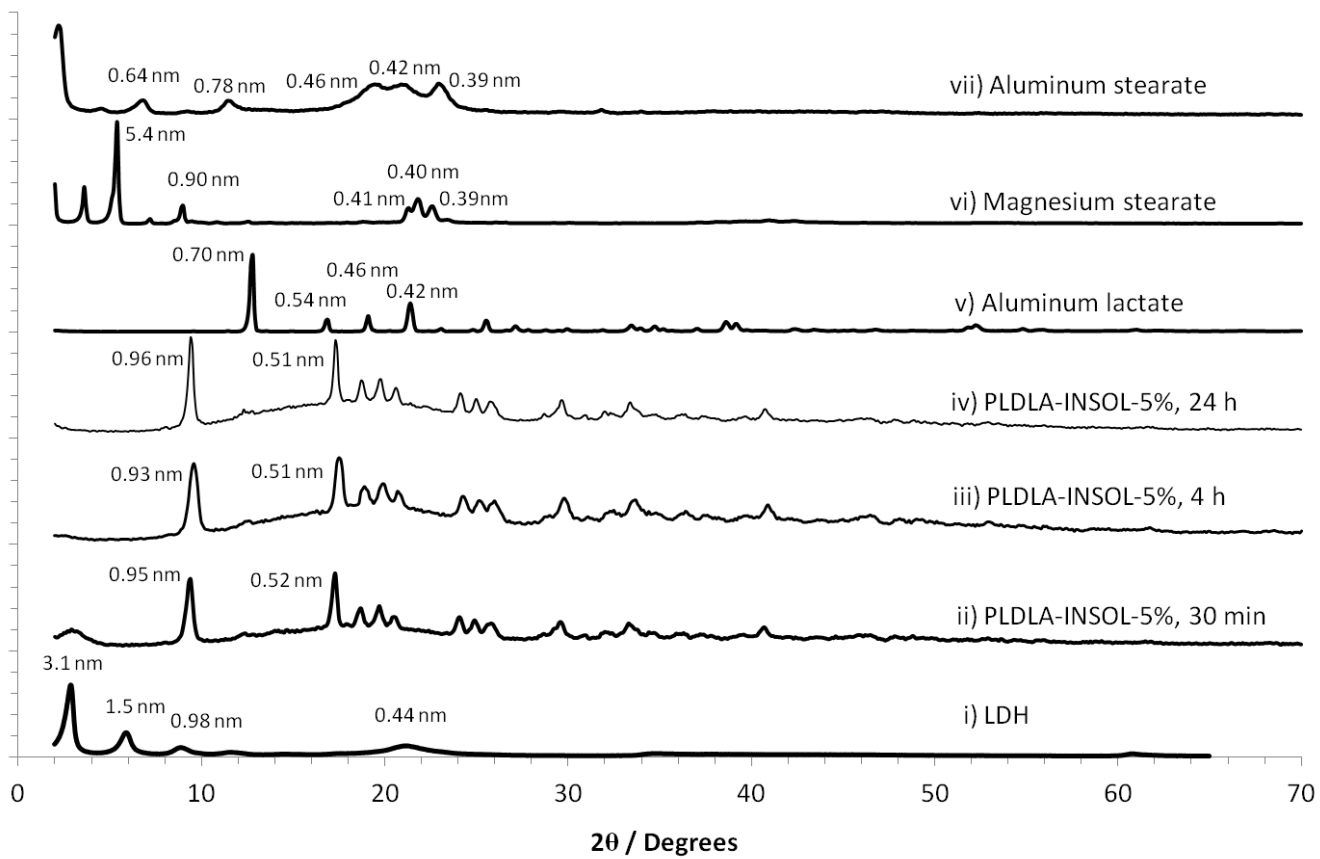
**Figure 16 Xray diffraction spectra of PLDLA-INSOL-5% compared with further control salts of aluminum and magnesium**
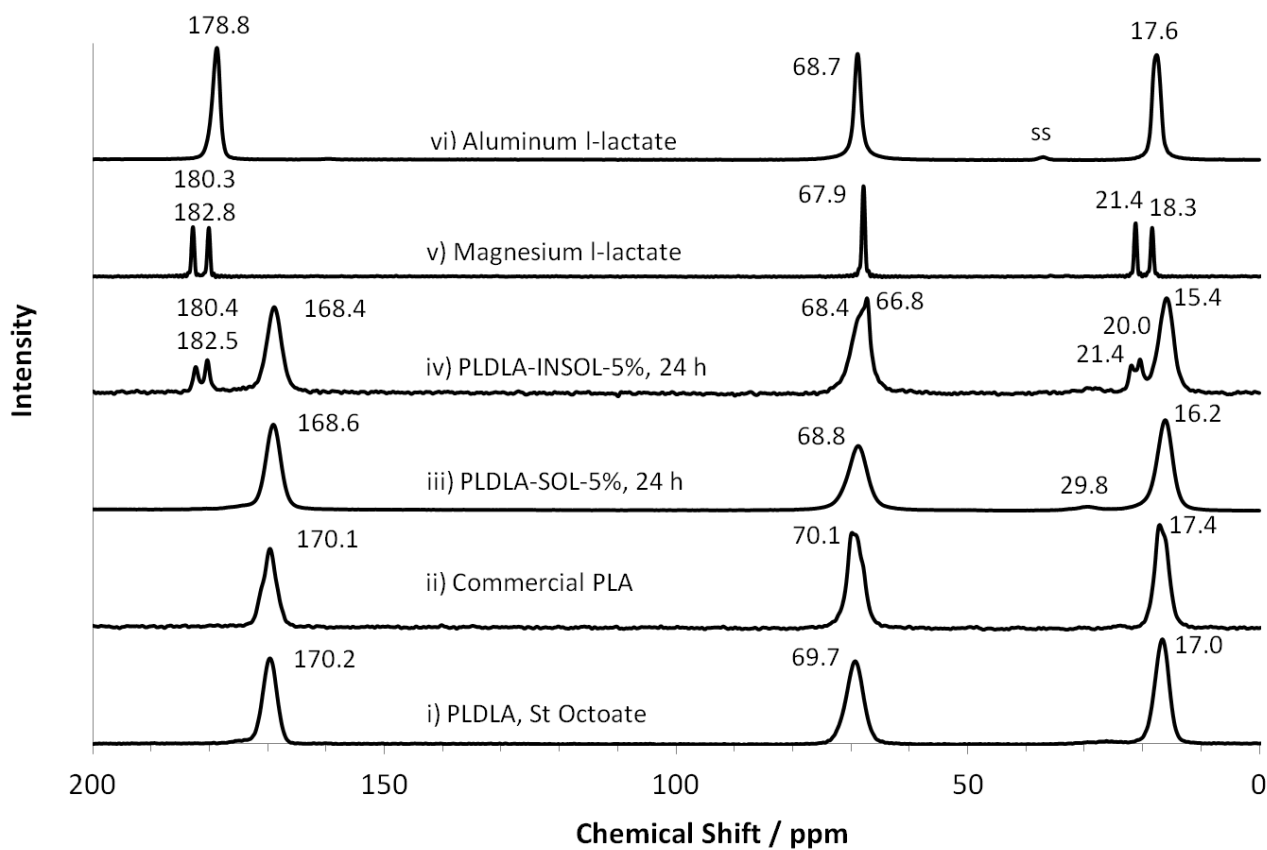
**Figure 17 Solid state $^{13}$C NMR of various species in PLDLA-LDH reaction system: i) PLDLA-1%-St-Oct, ii) Commercial PLDLA, iii) PLDLA-SOL-5%, iv) PLDLA-INSOL-5%, v) magnesium lactate, vi) aluminium lactate**

# Tables

**Table 1 Overall Polymer Mass Yield and Insoluble Residue Yield for PLDLA-HYB, (reaction time 24 h), at different LDH mass loadings, plus PLDLA-2.5%-Al-St, (Standard deviation = ± 2 % by mass)**

| Species | PLDLA-HYB Yield (% by mass) | Insoluble Fraction (% by mass) |
| --- | --- | --- |
| PLDLA-HYB-1% | 57.2 | 9.1 |
| PLDLA-HYB-5% | 88.5 | 24.4 |
| PLDLA-HYB-10% | 74.7 | 41.5 |
| PLDLA-HYB-15% | 73.5 | 34.3 |
| PLDLA-HYB-20% | 64.6 | 18.5 |
| PLDLA-2.5%-Al-St | 88.0 | 7.0 |

**Table 2 Bulk Elemental Analysis of PLDLA-HYB-5% Soluble and Insoluble Mass Fractions compared with original LDH: Inductively Coupled Plasma, ICP-OES, (% by mass), (Standard deviation = ± 5 %)**

| Species | LDH (% by mass) | PLDLA-HYB-5% | |
| --- | --- | --- | --- |
| | | PLDLA-INSOL-5% (% by mass) | PLDLA-SOL-5% (% by mass) |
| Mg | 11.30 | 8.46 | 0.39 |
| Al | 5.06 | 0.77 | 0.30 |
| **Mg: Al ratio** | **2.20** | **11.00** | **1.30** |